Check for updates

JOURNAL OF SANDWICH STRUCTURES & MATERIALS

Original Article

Journal of Sandwich Structures and Materials
0(0) 1–22
© The Author(s) 2020
Article reuse guidelines:
sagepub.com/journals-permissions
DOI: 10.1177/1099636220909792
journals.sagepub.com/home/jsm
SAGE

Free vibration and axial compression of all-metallic cylindrical and truncated conical sandwich shells with corrugated cores

Mao Yang[1], Bin Han[2,3], Peng-Bo Su[1], Zi-Han Wei[1], Qi Zhang[2], Qian-Cheng Zhang[1] and Tian Jian Lu[1,4]

Abstract

All-metallic sandwich-walled cylindrical and conical structures for aerospace applications often require simultaneous excellent vibration and load-carrying capacities. In the present study, the free vibration and axial compression behaviors of cylindrical and truncated conical sandwich shells with corrugated cores are investigated using a combined experimental and numerical approach. Excellent agreement between experimental measurements and finite element simulations for representative vibration and axial compression characteristics is achieved. Parametric studies based on the response surface model are subsequently performed to quantify the influence of key geometrical parameters on vibration and axial compression performance. A multi-functional collaborative design to meet the requirement of high load-bearing capacity subjected

[1]State Key Laboratory for Strength and Vibration of Mechanical Structures, Xi'an Jiaotong University, Xi'an, China
[2]School of Mechanical Engineering, Xi'an Jiaotong University, Xi'an, PR China
[3]Research Institute of Xi'an Jiaotong University, Hangzhou, China
[4]Nanjing Center for Multifunctional Lightweight Materials and Structures, Nanjing University of Aeronautics and Astronautics, Nanjing, PR China

Corresponding authors:
Bin Han, School of Mechanical Engineering, Xi'an Jiaotong University, Xi'an 710000, PR China.
Email: hanbinghost@mail.xjtu.edu.cn
Tian Jian, State Key Laboratory for Mechanical Structure Strength and Vibration of Mechanical Structures, Xi'an Jiaotong University, Xi'an 710000, PR China.
Email: tjlu@nuaa.edu.cn

to the constraint of low natural frequency is also carried out, which demonstrates the unique advantages of the novel sandwich-walled shells for aeronautical and astronautical applications.

Keywords

Free vibration, axial compression, cylindrical sandwich shell, truncated conical sandwich shell, corrugated core, optimization

Introduction

Cylindrical and conical structures have been widely used in aeronautical and astronautical applications, such as the fuselage sections of aircrafts, the interstages of launch vehicles, the fairing of rocket/aircrafts, and the rocket tail nozzles. These structures are often exposed to complex service conditions, e.g. severe vibration and axial impact [1–4]. For such applications, it is desirable to construct sandwich-walled cylindrical and conical structures (shells) sandwich structures are known to possess high specific strength, sound absorption performance, high designability, and good heat dissipation capability [5–13]. It is thus of great significance to investigate simultaneously the vibration and axial load-bearing capabilities of sandwich-walled cylindrical and conical shells with, for example, corrugated cores. Because the corrugated cores have fluid-through topologies, the sandwich-walled cylindrical and conical shells can also meet the increasingly pressing demand of active cooling in high temperature environments.

The vibration characteristics of sandwich-walled cylindrical and conical shells have rarely been explored, expect for a few studies on cylindrical sandwiches made of fiber-reinforced composites [14–18]. The free vibration of a carbon fiber-reinforced corrugated-core sandwich cylinder was found to fall mainly within the cross-sectional plane, and its fundamental frequency depends upon the circumferential bending stiffness of the sandwich wall [15]. Jiang et al. [16] fabricated an orthogrid sandwich cylinder via filament winding, and investigated its free vibration response using a combined experimental, theoretical, and numerical approach. The vibration damping of composite sandwich cylindrical shells with pyramidal truss-like cores have also been investigated [17,18]. However, for aeronautical and astronautical applications with high temperature environments, metallic materials are favored relative to the fiber-reinforced composites. Therefore, the study of all-metallic sandwich-walled cylindrical and conical shells is of great significance.

Similarly to free vibration, existing research on the axial compression behaviors of all-metallic sandwich-walled cylindrical and conical shells is rare. The stiffness and load capacity of carbon fiber-reinforced composite sandwich cylinders with Kagome cores were investigated, and it was found that the sandwich cylinder is stiffer and stronger by several times than a stiffened cylinder with similar dimensions and mass [19]. Li et al. [20] experimentally examined the strength and failure modes of a composite corrugated-core sandwich cylinder (CSC) subjected to uniaxial compression. It was demonstrated that the split forming method makes the CSC stiffer, while the method of integral filament winding forming makes the CSC stronger. The free vibration and uniaxial compression behaviors of composite orthogrid sandwich cylinders were investigated by Jiang et al. [16], although they did not consider the multi-functional collaborative design of the structure.

As for all-metallic sandwich cylindrical and conical shells, the cylindrical sandwich shells with corrugated cores (CSSCC) and truncated conical sandwich shells with corrugated cores (TCSSCC) have significant advantages in axial compression (peak strength, energy absorption, etc.) relative to their monolithic counterparts [21,22]. However, the free vibration behavior of these all-metallic sandwich constructions is yet studied. Further, the collaborative design of CSSCC and TCSSCC for simultaneous high load-bearing and free vibration performance needs to be studied.

In the current study, all-metallic CSSCC and TCSSCC are fabricated. Tests for free vibration and quasi-static axial compression are subsequently carried out. Next, full three-dimensional (3D) finite element (FE) models are developed to predict the modal characteristics of the CSSCC and TCSSCC. Systematic parametric studies based on the response surface model (RSM) are also carried out to explore the influence of key geometrical parameters of the sandwich structure on free vibration and axial compression characteristics. Finally, the collaborative design of CSSCC and TCSSCC for high loading-bearing capacity subjected to the constraint of low natural frequency is carried out.

Experiments

Fabrication methodology

The fabrication procedures for CSSCC and TCSSCC test samples can be divided into four main steps, as illustrated in Figure 1 [21,22]. Firstly, the corrugated (folded) plate (shown in red) is processed via stamping (Figure 1(a)); secondly, shape correction of the corrugated core is achieved by molding (Figure 1(b)); thirdly, the outer and inner face shells (shown in chartreuse and orange, respectively) are fabricated (Figure 1(c)); finally, the inner face shell, the outer face shell and the corrugated core are assembled and connected together, with all the interfaces tied by epoxy adhesive (LOCTITE Hysol E-120HP). Both the core and the face shell are made of aluminum 1060Al, with the uniaxial tensile stress versus strain curve shown in Figure 2.

Table 1 summarizes the geometrical parameters of the CSSCC and TCSSCC samples shown in Figure 3. For the CSSCC, the inner radius $R_{\mathrm{i}} = 57\,\mathrm{mm}$, the outer radius $R_{\mathrm{o}} = 67.5\,\mathrm{mm}$, the width of corrugated core $w = 2\,\mathrm{mm}$, the height of sandwich shell $h = 145\,\mathrm{mm}$, and the number of circumferential corrugations $N = 20$, are chosen as the invariable parameters. For the TCSSCC, the inner radius of the small end $R_{\mathrm{i-u}} = 57.7\,\mathrm{mm}$, the outer radius of the small end $R_{\mathrm{o-u}} = 66.67\,\mathrm{mm}$, the inner radius of the big end $R_{\mathrm{i-d}} = 94.97\,\mathrm{mm}$, the outer

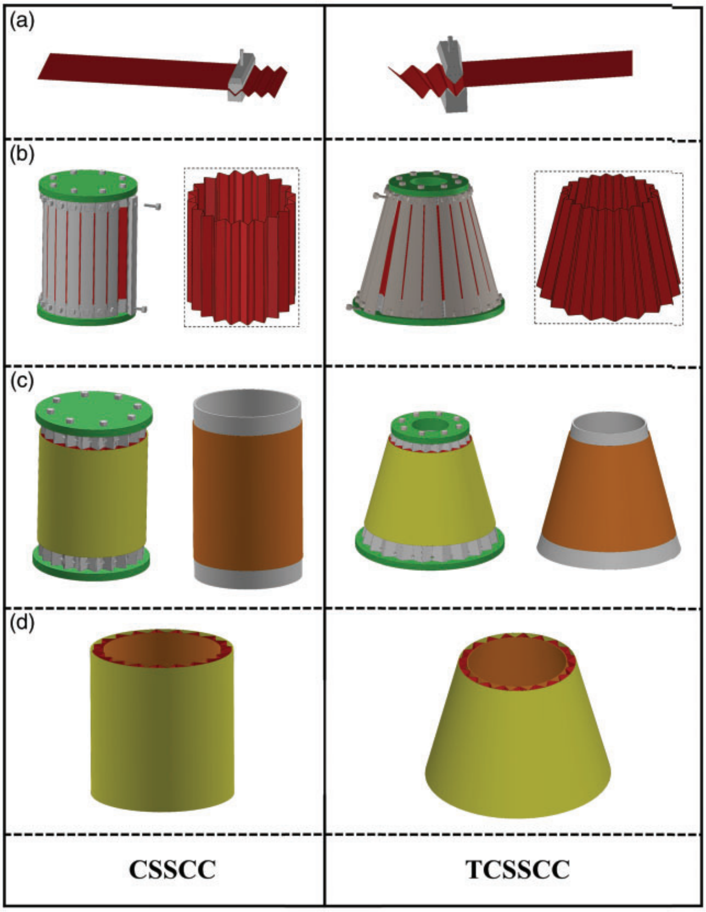

Figure 1. Mold design and fabrication processes for CSSCC and TCSSCC: (a) fabricating the corrugated plate, (b) shape correction of corrugated core, (c) fabricating the face sheets, and (d) assembling. The corrugated core is shown by red, the outer face by chartreuse, and the inner face by orange.
CSSCC: cylindrical sandwich shells with corrugated cores; TCSSCC: truncated conical sandwich shells with corrugated cores.

radius of the big end $R_{o-d} = 104.92\,\text{mm}$, the semi-apical angle $\theta = 14.87°$; the remaining parameters are identical to those of the CSSCC: $w = 2\,\text{mm}$, $h = 145\,\text{mm}$, and $N = 20$.

Modal testing

To reveal the characteristics of free vibration for both the CSSCC and TCSSCC samples, modal tests are performed under free-free boundary condition. The

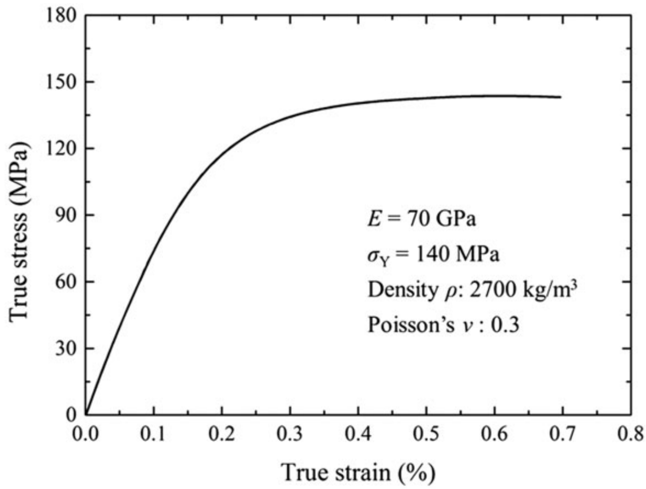

Figure 2. Measured tensile stress versus strain curve for 1060Al.

Table 1. Parameters of CSSCC and TCSSCC test samples.

	t_o (mm)	t_c (mm)	t_i (mm)	Total mass (g)	Mass of epoxy resin (g)
CSSCC_212	0.2	0.1	0.2	93.15	7.11
				91.82	6.23
CSSCC_424	0.4	0.2	0.4	177.30	5.54
				175.75	3.91
TCSSCC_424	0.4	0.2	0.4	229.57	12.57
				231.24	14.24
TCSSCC_444	0.4	0.4	0.4	283.12	14.12
				285.02	16.02

CSSCC: cylindrical sandwich shells with corrugated cores; TCSSCC: truncated conical sandwich shells with corrugated cores.

experimental set-up and specimens are shown in Figure 4, with the samples suspended by elastic ropes to most closely simulate free–free boundary condition. The addition of the elastic rope adds a weak constraint to the structure, which would result in a slightly higher natural frequency. However, the effect of the elastic rope is quite small and can be ignored. This method has been confirmed to be feasible to simulate the free-free boundary condition [16,23]. An impact hammer, a B&K type accelerometer, a charge amplifier and a LMS-Test-Lab modal analysis system are used to perform the experiments, as shown in Figure 4. There are 50 input points and a single testing point on each sample. First, the force hammer with a sensitivity

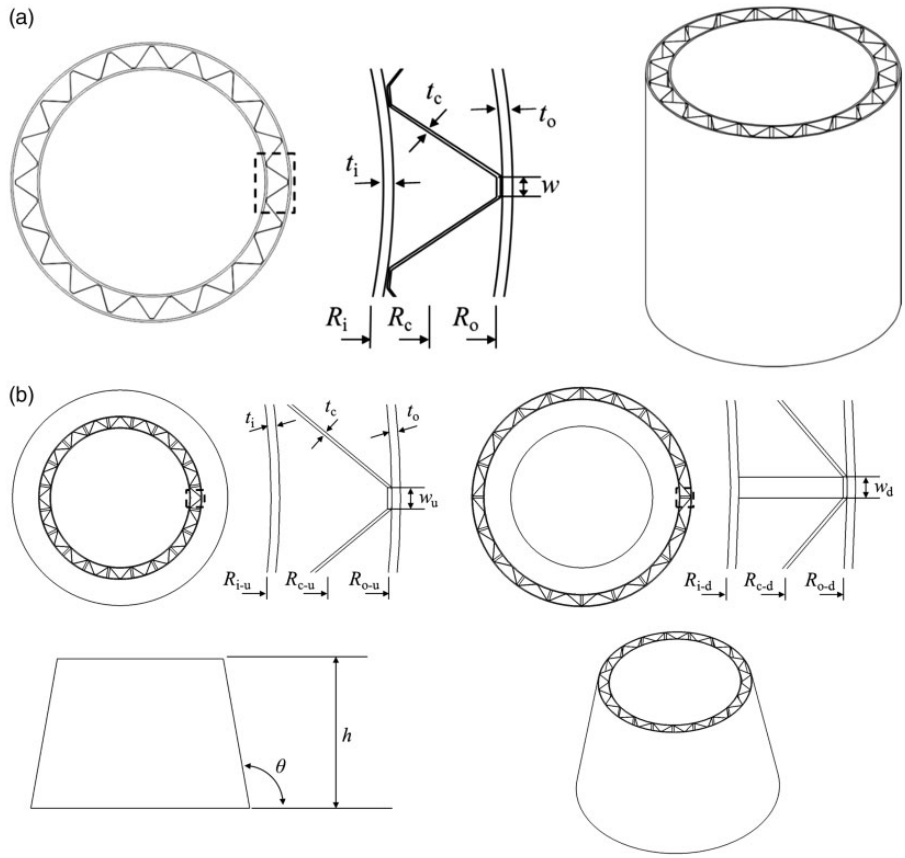

Figure 3. Geometric parameters of (a) CSSCC and (b) TCSSCC.
CSSCC: cylindrical sandwich shells with corrugated cores; TCSSCC: truncated conical sandwich shells with corrugated cores.

of 2.24 mV/N is employed to tap the input points, with each point taped 5 times. The vibratory response is measured using the acceleration transducer with a sensitivity of 100 mV/g. Testing signals are processed with the LMS-Test-Lab modal analysis system. The first three natural frequencies and the corresponding mode shapes are obtained for each test sample. Figure 5 presents typical frequency response functions measured for both samples.

Axial compression testing

Similar to our previous work [22], quasi-static axial compression tests are carried out with a hydraulic testing machine (MTS) at ambient temperature, as shown in Figure 6. The bottom platen of the machine is fixed, while the top platen is moved

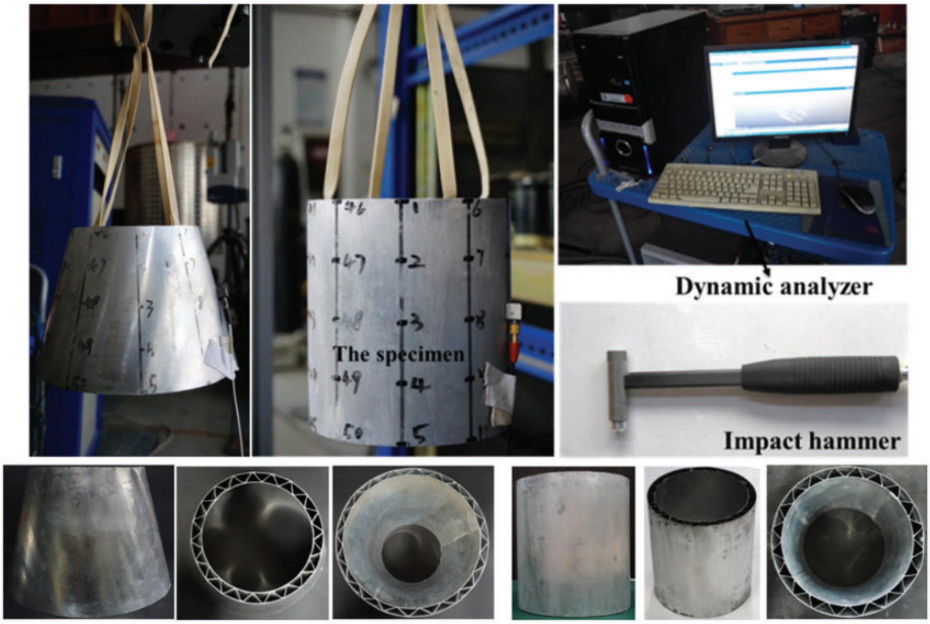

Figure 4. Test setup of modal testing and specimens.

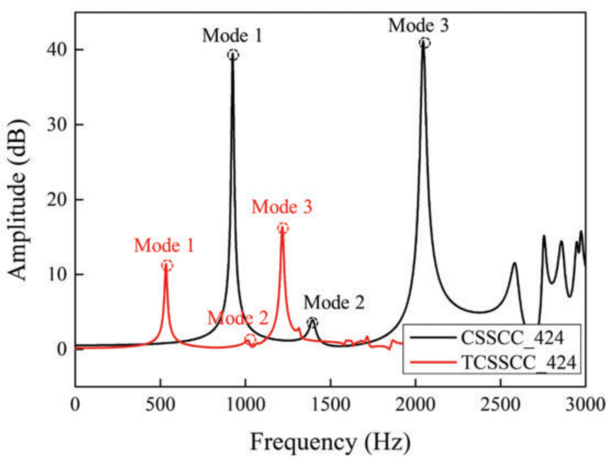

Figure 5. Typical frequency response functions of CSSCC and TCSSCC.
CSSCC: cylindrical sandwich shells with corrugated cores; TCSSCC: truncated conical sandwich shells with corrugated cores.

Figure 6. Axial compression test.

axially downward to compress the CSSCC/TCSSCC samples, with the speed fixed at 1.0 mm/min and the compression distance at 50 mm. During the compression tests, load and displacement data are obtained using a computer-based data acquisition system. In the current study, the first maximum value of the axial force during compression (peak force, PF) is taken as the axial loading capacity of the sample.

FE modeling and validation

Modeling details

The vibration characteristics of CSSCC and TCSSCC are further analyzed using the method of FE with the commercial FE code ABAQUS/Standard. Linear perturbation analysis based upon the Lanczos Eigensolver is applied to extract the natural frequencies and mode shapes. Linear quadrilateral shell elements with

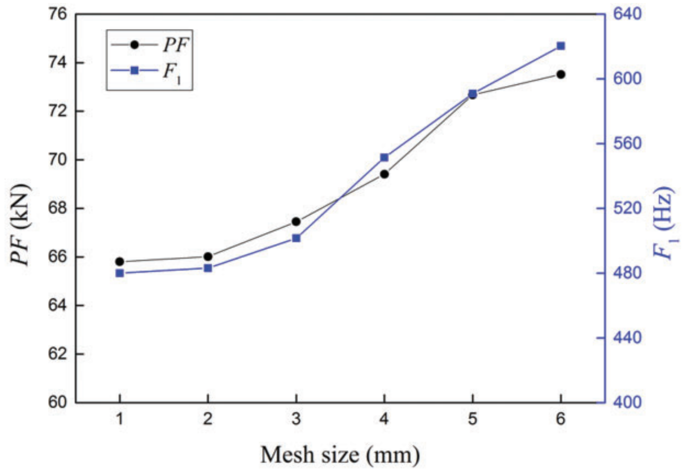

Figure 7. Mesh sensitivity of PF and F_1.
PF: peak force.

induced integration (S4R) are used for both the face sheets and the corrugated plate, with mesh convergence carefully considered and guaranteed for each calculation. Figure 7 presents the sensitivity of first natural frequency (F_1) and PF to of TCSSCC to the mesh size. It is implied that the convergence of the calculations can be guaranteed when the mesh size is <2 mm. For all the later simulations, the mesh size is set to 2 mm. All the interfaces are assumed to be perfectly bonded, and the boundary condition is set as free.

The PF of the CSSCC and TCSSCC under axial compression is extracted from 3D FE simulations. For both sandwich-walled shells, the geometrical parameters selected are identical to those of the test samples. The material properties are the same as those listed in Figure 1. Both the face sheets and the corrugated core are modeled using 4-node shell elements (S4R), with five-integration points through the thickness [24]. Two rigid plates are used to model the puncher. For all the FE simulations, the bottom rigid plate is constrained in all degrees of freedom, whereas the top rigid plate is fixed in all translational and rotational degrees of freedom except for a slow axial velocity to ensure quasi–static compression. General contact is applied for the entire model, with a Coulomb friction coefficient of 0.2.

Validation and analysis

The first three natural frequencies and the corresponding vibration mode shapes of CSSCC and TCSSCC obtained by experiments and FE simulations are compared, as shown in Table 2 and Figure 8, and good agreement in term of both natural frequencies and mode shapes is achieved. For the CSSCC, the first vibration mode is the oval lobar mode, the second mode is the twisting oval lobar mode, and the third mode is

Table 2. The first three natural frequencies by FEM and experimental method of (a) CSSCC and (b) TCSSCC.

	The first three natural frequencies (Hz)		
	1	2	3
CSSCC_424			
FEM	1083	1629	2282
EXP			
1	925	1396	2038
2	955	1460	2146
CSSCC_212			
FEM	557	976	1107
EXP			
1	570	1016	1207
2	565	1008	1195
TCSSCC_444			
FEM	480	1129	1161
EXP			
1	539	1036	1082
2	536	1035	1080
TCSSCC_424			
FEM	478	1079	1089
EXP			
1	533	1020	1073
2	537	1035	1099

CSSCC: cylindrical sandwich shells with corrugated cores; TCSSCC: truncated conical sandwich shells with corrugated cores.

the triangle lobar mode. For the TCSSCC, the first mode is the oval lobar mode, the second is the triangle lobar mode, and the third is the twisting oval lobar mode.

Comparison of the PF obtained from both the experiments and FE simulations are compared, as listed in Table 3. The force–displacement curves of TCSSCC_444 specimens from both numerical simulations and experimental measurement are compared in Figure 9. Again, good agreement is achieved. More details are described in our previous research [21,22].

Optimization

In practical applications, a structure is often required to satisfy simultaneous vibration and load-carrying requirements. For instance, its PF should be high enough, while its natural frequency needs to be limited within a certain range. Due to the geometrical complexity of CSSCC and TCSSCC and the nonuniformity along the axial direction of TCSSCC, it is difficult to acquire the vibration characteristics of the CSSCC and TCSSCC via the theoretical method route. In the

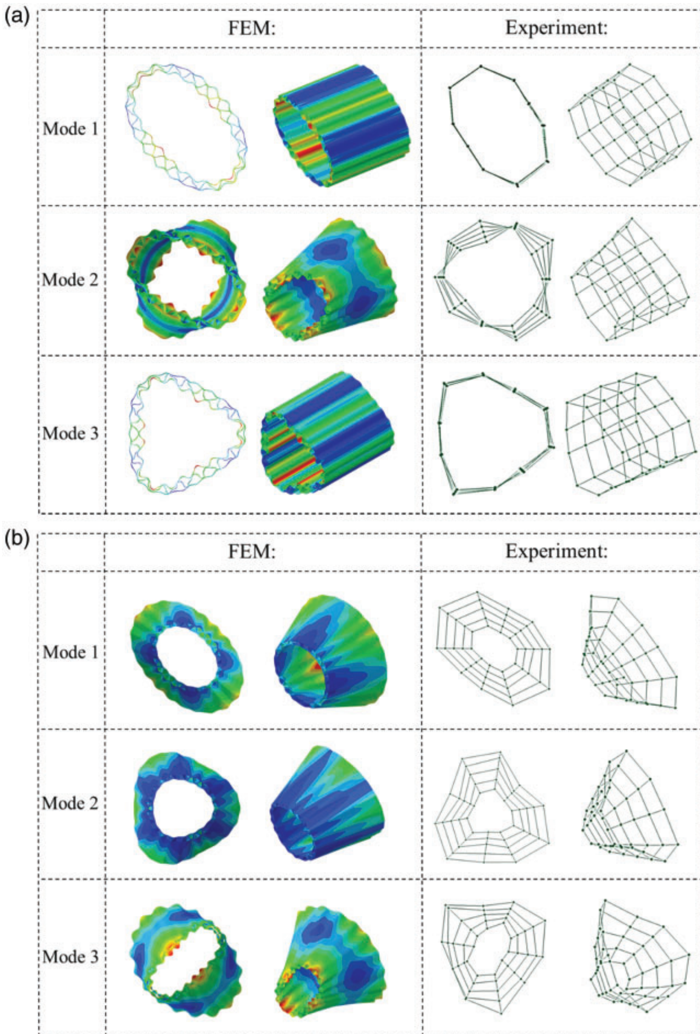

Figure 8. Mode shapes of (a) CSSCC and (b) TCSSCC obtained by FE simulations and experimental measurements.
CSSCC: cylindrical sandwich shells with corrugated cores; FE: finite element; TCSSCC: truncated conical sandwich shells with corrugated cores.

present study, the design of experiments (DOE) approach is adopted to obtain expressions for both the first natural frequency (F_1) and PF. Based upon the DOE, optimization is performed to acquire the maximum load carrying capacity (i.e. PF), while the first natural frequency is limited to a specific range.

In this section, the thicknesses of the shell faces and corrugated plate (t_o, t_i, and t_c; Figure 3) are assumed to vary from 0.2 mm to 1.0 mm for both CSSCC and

Table 3. Comparison between FE simulations and experimental measurements for the PF.

	PF		
Specimens	FEM (kN)	Experiment (kN)	Error (%)
CSSCC_424	13.1	12.9	1.6
CSSCC_212	41.1	34.9	17.8
TCSSCC_444	44.6	37.2	16.5
TCSSCC_424	66.1	58.3	11.8

CSSCC: cylindrical sandwich shells with corrugated cores; FE: finite element; PF: peak force; TCSSCC: truncated conical sandwich shells with corrugated cores.

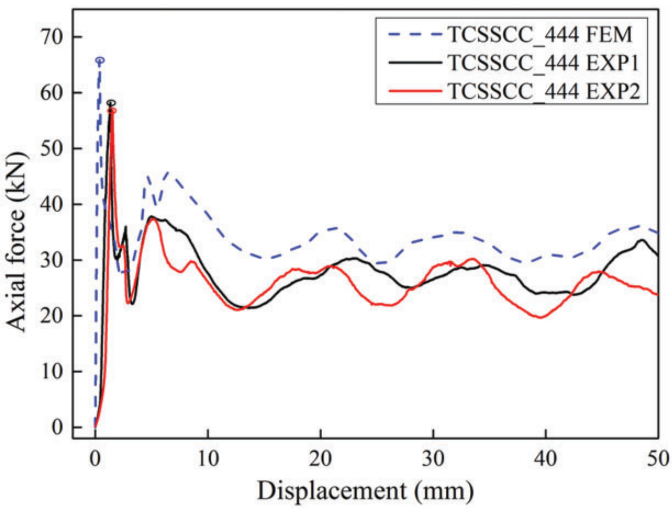

Figure 9. Comparison of axial force–displacement curves from both numerical simulation and experimental measurement.

TCSSCC. Specifically, $R_i = 57\,\text{mm}$, $R_o = 67.5\,\text{mm}$, $w = 2\,\text{mm}$, $h = 145\,\text{mm}$, and $N = 20$ are chosen to be the same as those of experimental sample for CSSCC; while $R_{i-u} = 57.7\,\text{mm}$, $R_{o-u} = 66.67\,\text{mm}$, $R_{i-d} = 94.97\,\text{mm}$, $R_{o-d} = 104.92\,\text{mm}$, $w = 2\,\text{mm}$, $\theta = 14.87^\circ$, $h = 145\,\text{mm}$, and $N = 20$ are the same as those of the experimental sample for TCSSCC.

RSM for free vibration

Firstly, the Latin hypercube design (LHD), which has powerful capacity in nonlinear modeling and good prediction with little sampling points [25], is adopted to obtain the experimental design points, and 35 design points are selected.

Table 4. Sample points and relevant numerical F_1 results on these points.

				CSSCC	TCSSCC
Number	t_o (mm)	t_i (mm)	t_c (mm)	F_1 (Hz)	F_1 (Hz)
1	0.72	0.80	0.75	1509.8	707.76
2	0.69	0.21	0.37	674.16	302.29
3	0.21	0.45	0.53	661.75	294.23
4	0.83	0.27	0.72	813.19	368.66
5	0.59	0.29	0.91	848.15	385.68
6	0.35	0.93	0.99	955.13	433.18
7	0.45	0.77	0.59	1245.4	568.11
8	0.40	0.48	0.21	1126.9	504.33
9	0.88	0.96	0.24	1606.2	793.75
10	0.91	0.24	0.40	732.34	329.6
11	0.43	0.56	0.88	1119.2	508.71
12	0.93	0.53	0.35	1298.1	597.96
13	0.96	0.88	0.83	1626.2	775.34
14	0.37	0.91	0.29	1114.1	498.73
15	0.77	0.37	0.96	1037.9	473.48
16	0.24	0.61	0.45	765.31	417.76
17	0.29	0.59	0.27	951.73	689.35
18	0.75	0.69	0.32	1463.3	689.35
19	0.67	0.83	0.69	1492.7	698.59
20	0.99	0.85	0.56	1618.8	773.36
21	0.53	0.43	0.48	1164.7	524.66
22	0.27	0.75	0.85	769.97	346.98
23	0.80	0.72	0.67	1507.9	705.79
24	0.85	0.35	0.61	1034.8	468.35
25	0.61	0.32	0.93	920.79	418.62
26	0.56	0.64	0.43	1354.5	621.9
27	0.64	0.99	0.80	1484	696.04
28	0.48	0.51	0.77	1176.3	534.74
29	0.51	0.67	0.51	1319.1	603.38
30	0.32	0.40	0.64	910.95	408.17
31	0.60	0.28	0.28	855.62	382.44
32	0.76	0.44	0.92	1182.2	540.83
33	0.28	0.60	0.76	824.77	370.42
34	0.92	0.76	0.44	1548.2	734.32
35	0.44	0.92	0.60	1225	559.6

CSSCC: cylindrical sandwich shells with corrugated cores; TCSSCC: truncated conical sandwich shells with corrugated cores.

The design points and the numerical simulation results of F_1 are listed in Table 4. Subsequently, approximation functions are fitted using the multiple regression fitting method, with the full third-order set of polynomial functions employed as the basis function. By fitting these data, response surface functions of F_1 are obtained for both CSSCC and TCSSCC, as listed in Appendix 1.

Table 5. Accuracy evaluation of the RSM.

		R^2	P	R^2_{adj}
CSSCC	F_1	0.999	0.000	0.999
TCSSCC	F_1	0.970	0.000	0.970

CSSCC: cylindrical sandwich shells with corrugated cores; RSM: response surface model; TCSSCC: truncated conical sandwich shells with corrugated cores.

To evaluate accuracy of the RSM, certain indicators are studied: the R square values (R^2), the adjusted square error (R^2_{adj}), and the P-value. Their normalized expressions are given by

$$\begin{aligned} RMSE &= 1 - SSE/SST, \quad SST = \sum_{i=1}^{N} (y_i - \bar{y}_{\text{i}})^2 \\ R^2_{\text{adj}} &= 1 - (1 - R^2)\frac{N-1}{N-p-1} \end{aligned} \tag{1}$$

where y_i represents the FE solution; $\bar{y}_{\text{i}}(x)$ is the mean value of y_i; SSE and SST are the sum of squared errors and the total sum of squares; and P is the number of non-constant terms in the RSM. The value of R^2, R^2_{adj}, and P are calculated and summarized in Table 5. Note that each model is required to satisfy the condition that the values of R^2 and R^2_{adj} are >0.9, while the value of P does not exceed 0.05.

Next, parameters study based on the RSM are carried out to quantify the influence of t_{o}, t_i, and t_c on the first natural frequency F_1, as shown in Figure 10. To this end, when one thickness is varied, the other two are fixed at 0.5 mm. The F_1 of either CSSCC or TCSSCC is seen to increase with increasing t_{o} or t_i in the range of 0.2–1.0 mm. In contrast, F_1 is not sensitive to t_c for both CSSCC and TCSSCC: actually, F_1 slightly decreases as t_c is increased. This is because that the first vibration mode has the oval lobar shape for both CSSCC and TCSSCC, which implies that the first-order vibration of these structures is dominated by bending. The bending deformation of the sandwich structure is mainly determined by its face sheets while the shearing deformation is mainly dependent on the sandwich core. The core has little effect on the bending stiffness. Therefore, increasing the thickness of the face sheets (t_{o}, t_i) will increase the bending stiffness of the structure, thus increasing the F_1. Increasing the thickness of the core plate (t_c) could not lead to a dramatic improvement on the bending stiffness, but would increase the mass of the structure, and hence F_1 is somewhat reduced.

To further validate the RSM, the corresponding FE results are presented in Figure 10 (red squares). Excellent agreement between the FE results and the RSM predictions is achieved.

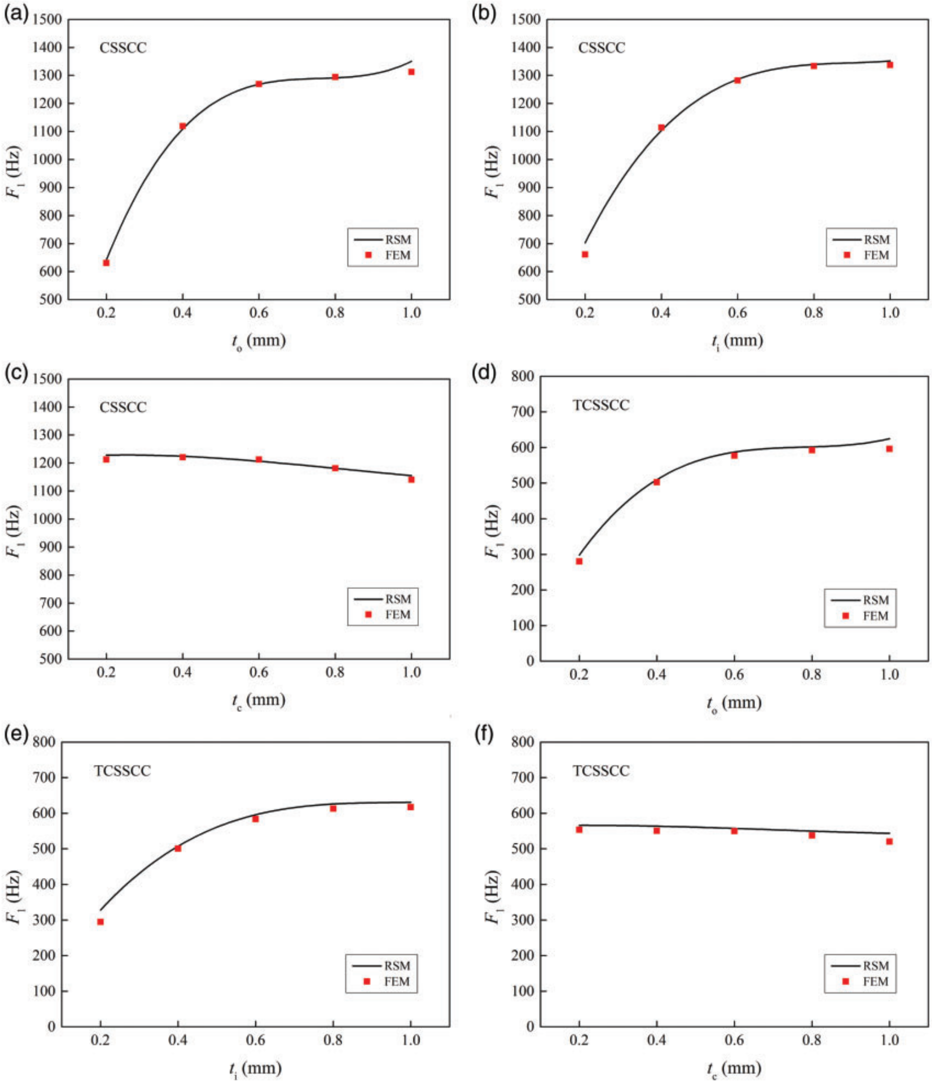

Figure 10. Effects of t_o, t_i, and t_c on the first natural frequencies of CSSCC and TCSSCC. CSSCC: cylindrical sandwich shells with corrugated cores; TCSSCC: truncated conical sandwich shells with corrugated cores.

RSM for axial compression

Similarly, for the PF analysis, 36 design points are selected as the experimental design points in the LHD. The design points and FE simulation results of PF are summarized in Table 6. The approximation functions are fitted using the method

Table 6. Sample points and relevant numerical PF results on these points.

				CSSCC	TCSSCC
Number	t_o (mm)	t_i (mm)	t_c (mm)	PF (kN)	PF (kN)
1	0.84	0.90	0.93	178.30	199.47
2	0.80	0.86	0.46	132.59	150.23
3	0.34	0.29	0.78	97.18	102.01
4	0.86	0.59	0.76	148.31	164.98
5	0.57	0.50	0.51	101.48	110.36
6	0.29	0.70	0.65	104.76	115.01
7	0.48	0.74	0.25	81.29	89.43
8	0.99	0.80	0.82	172.86	195.44
9	0.42	0.76	0.95	143.28	156.29
10	0.91	0.23	0.34	93.47	104.19
11	0.88	0.21	0.69	120.49	132.45
12	0.70	0.95	0.23	104.30	120.20
13	0.44	0.61	0.38	86.46	93.55
14	0.90	0.36	0.84	145.62	158.89
15	0.72	0.82	0.48	126.71	141.95
16	0.59	0.53	0.40	95.07	104.02
17	0.23	0.78	0.67	106.61	119.44
18	0.78	0.93	0.44	133.21	151.08
19	0.93	0.99	0.70	168.36	191.95
20	0.69	0.63	0.72	135.08	148.83
21	0.74	0.30	0.74	122.56	133.32
22	0.67	0.27	0.55	99.65	107.60
23	0.40	0.34	0.30	61.96	65.63
24	0.55	0.88	0.42	112.04	124.75
25	0.46	0.42	0.91	123.73	132.59
26	0.65	0.84	0.36	111.60	125.59
27	0.25	0.38	0.88	104.83	111.76
28	0.38	0.97	0.61	122.30	136.27
29	0.36	0.51	0.99	128.87	138.14
30	0.76	0.32	0.53	107.01	117.60
31	0.63	0.65	0.32	96.55	108.24
32	0.50	0.57	0.97	139.93	151.14
33	0.82	0.44	0.21	84.26	96.35
34	0.27	0.91	0.80	126.80	142.50
35	0.61	0.69	0.86	145.25	158.48
36	0.51	0.67	0.90	140.24	152.21

CSSCC: cylindrical sandwich shells with corrugated cores; PF: peak force; TCSSCC: truncated conical sandwich shells with corrugated cores.

of multiple regressions fitting, with the full third-order set of polynomial functions are adopted as the basis function. By fitting these data, the response surface functions of PF are obtained, as list in Appendix A. Corresponding values of R^2, R^2_{adj}, and P are summarized in Table 7. Each model satisfies the condition that R^2 and R^2_{adj} have values >0.9, and the value of P is <0.05.

Table 7. Accuracy evaluation of the RSM.

	R^2	P	${R_{adj}}^2$
PF			
CSSCC	0.999	0.000	0.999
TCSSCC	0.999	0.000	0.999

CSSCC: cylindrical sandwich shells with corrugated cores; PF: peak force; RSM: response surface model; TCSSCC: truncated conical sandwich shells with corrugated cores.

The influence of various thicknesses (t_o, t_i, t_c) on PF is shown in Figure 11: when one thickness is varied, the other two are fixed at 0.5 mm. It is seen that the PF of CSSCC or TCSSCC increases dramatically with the increase of t_o, t_i, or t_c. To further verify the correctness of the RSM, Figure 11 presents the corresponding FE results (red squares), with excellent agreement obtained between FE results, and model predictions.

Optimization of free vibration and axial compression

As previously mentioned, for certain applications, it is advantageous for the CSSCC or TCSSCC to possess a high load carrying capacity (i.e. PF), while restricting its first natural frequency to a specific range. Therefore, in the current section, optimization is carried out by selecting the PF as the objective function and F_1 as a constraint, as follows

$$\begin{aligned} &\mathrm{Max}(PF); \\ &s.t.: 0.2 \le t_o,\ t_i,\ t_c \le 1.0\,\mathrm{mm} \\ &s.t.: F_{\mathrm{lower}} \le F_1 \le F_{\mathrm{upper}} \end{aligned} \tag{2}$$

where F_{lower} and F_{upper} are separately the lower and upper bounds of F_1. The above optimization problem can be solved using the sequential quadratic programming algorithm coded in MATLAB. It is noticed that that the upper (1700 or 1000 Hz) and lower (400 or 100 Hz) boundaries of the total frequency range are determined by the selected range of panel thicknesses (t_o, t_i, and t_c). The maximum PF (marked as MaxPF in Figure 12) of the structure is obtained by optimization, with its F_1 restricted to a specific allowable range. At the same time, to further reflect the optimization effect and the designability of CSSCC and TCSSCC, the minimum PF (marked as MinPF in Figure 12) is also calculated via optimization, with F_1 within the allowable range. Thus, the extent to which the PF is increased by optimization can be obtained, that is, $(\mathrm{Max}PF - \mathrm{Min}PF)/\mathrm{Min}PF$.

From Figure 12(a), for the CSSCC, it is seen that the increase of PF by optimization is significant. Especially, with F_1 in the range of 500–600 Hz, the optimized PF can be increased by 379%. With F_1 in the range of 1600–1700 Hz, the increase rate of PF is smallest and the optimized PF can be increased by 100%.

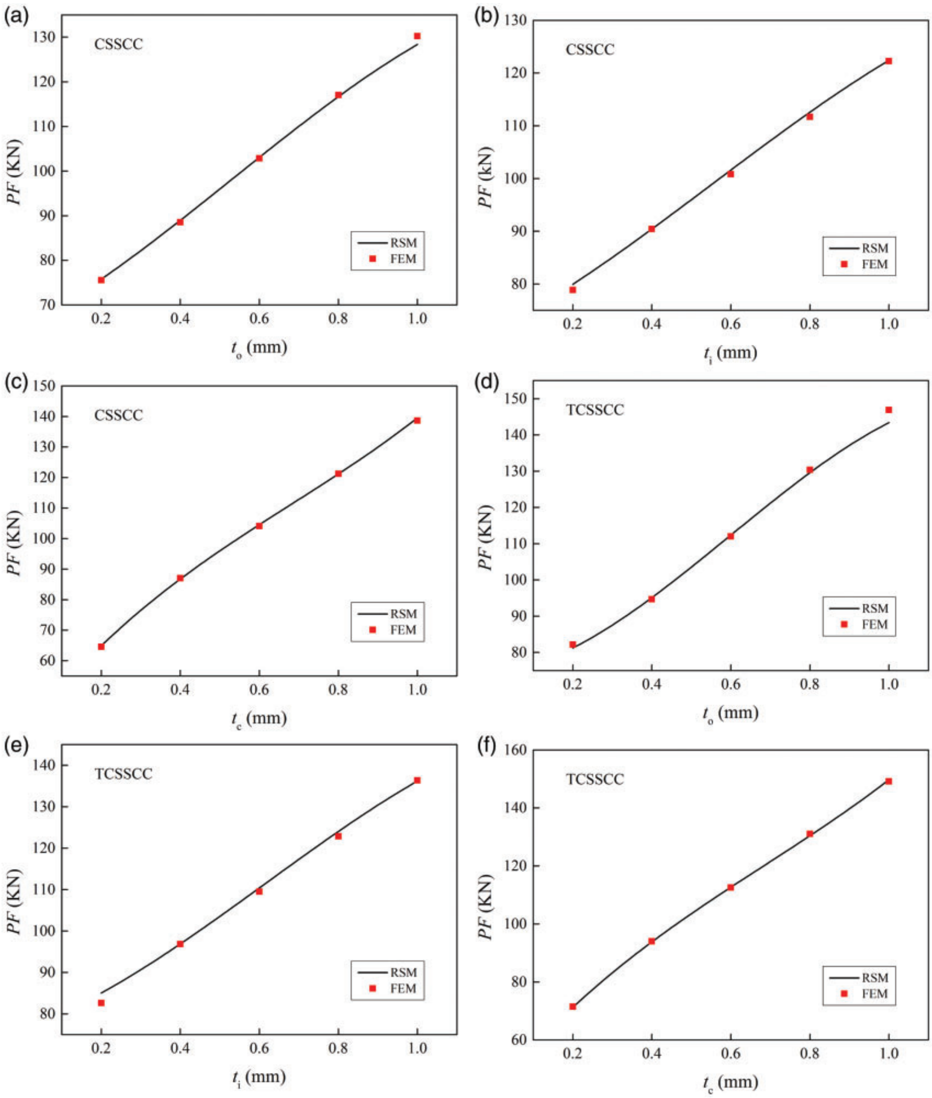

Figure 11. Effects of t_o, t_i, and t_c on the PF (peak force) of CSSCC and TCSSCC. CSSCC: cylindrical sandwich shells with corrugated cores; PF: peak force; TCSSCC: truncated conical sandwich shells with corrugated cores.

From Figure 12(b), for the TCSSCC, the optimized PF is also seen to increase as the constraint of F_1 is increased. Especially, with F_1 limited within the range of 200–300 Hz, the optimized PF can be increased by 495%. In comparison, when F_1 is limited within the range of 950–1050 Hz, the increase rate of PF is the smallest and the optimized PF is increased by only 64%.

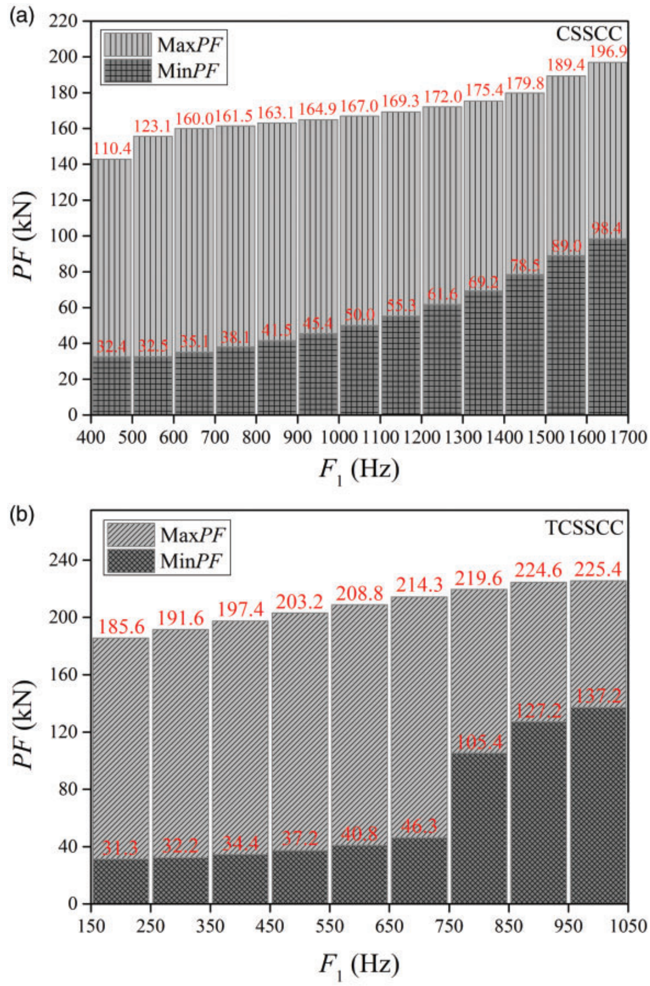

Figure 12. The PF (a) CSSCC and (b) TCSSCC obtained within selected nature frequency ranges.
CSSCC: cylindrical sandwich shells with corrugated cores; PF: peak force; TCSSCC: truncated conical sandwich shells with corrugated cores.

Conclusions

The free vibration and axial compression behaviors of cylindrical and truncated conical sandwich-walled shells with corrugated cores are investigated both experimentally and numerically. Numerical simulations results with the method of FEs agree well with those measured experimentally. RSM of the first natural frequency F_1 and peak force PF for each type of structure are established using the multivariate regression method. Detailed parametric studies based on the RSM are subsequently carried out to explore the influences of key geometrical parameters of the sandwich structure on F_1 and PF. Finally, optimization of the structure is carried out by selecting the PF as the objective function and F_1 as a constraint. It is demonstrated that the load carrying capacity (i.e. peak force) of either cylindrical or truncated conical sandwich-walled shell can be dramatically increased via optimization when the first natural frequency is required to fall within a specific range.

Declaration of Conflicting Interests

The author(s) declared no potential conflicts of interest with respect to the research, authorship, and/or publication of this article.

Funding

The author(s) disclosed receipt of the following financial support for the research, author ship, and/or publication of this article. This work is supported by the National Natural Science Foundation of China (11802221 and 51875441), the National Key R&D Program of China (2018YFB1106400), the China Postdoctoral Science Foundation (2016M600782), the Postdoctoral Scientific Research Project of Shaanxi Province (2016BSHYDZZ18), the Zhejiang Provincial Natural Science Foundation of China (LGG18A020001), Natural Science Basic Research Plan in Shaanxi Province of China (2018JQ1078), and the Open Fund of the State Key Laboratory of Mechanics and Control of Mechanical Structures (MCMS-I-0219K01 and MCMS-E-0219K02), China.

ORCID iD

Mao Yang https://orcid.org/0000-0002-0062-2446

References

1. Kerboua Y and Lakis AA. Numerical model to analyze the aerodynamic behavior of a combined conical-cylindrical shell. *Aerosp Sci Technol* 2016; 58: 601–617.
2. Hilburger MW. On the development of shell buckling knockdown factors for stiffened metallic launch vehicle cylinders. *NASA Technical Note*, TM-2018-23681.
3. Bouazizi M, Lazghab T and Soula M. Mechanical response of a panel section with a hexagonally tessellated stiffener grid. *P I Mech Eng G-J Aer Eng* 2016; 231: 1402–1414.
4. Gene C and Schultz MR. Buckling analysis of a honeycomb-core composite cylinder with initial geometric imperfections. *NASA Technical Note*, TM–2013-217967.
5. Cote F, Deshpande VS, Fleck NA, et al. The out-of-plane compressive behavior of metallic honeycombs. *Mater Sci Eng A* 2004; 380: 272–280.
6. Yan LL, Yu B, Han B, et al. Effects of aluminum foam filling on the low-velocity impact response of sandwich panels with corrugated cores. *J Sandwich Struct Mater*. Epub ahead of print 22 May 2018. DOI: 10.1177/1099636218776585.
7. Yan LL, Yu B, Han B, et al. Compressive peak force and energy absorption of sandwich panels with aluminum foam-filled corrugated cores. *Compos Sci Technol* 2013; 86: 142–148.

8. Cheng Y, Zhou T, Wang H, et al. Numerical investigation on the dynamic response of foam-filled corrugated core sandwich panels subjected to air blast loading. *J Sandwich Struct Mater* 2019; 21: 838–864.
9. Han B, Qin KK, Yu B, et al. Honeycomb-corrugation hybrid as a novel sandwich core for significantly enhanced compressive performance. *Mater Des* 2016; 93: 271–282.
10. Khalkhali A, Khakshournia S and Nariman-Zadeh N. A hybrid method of FEM, modified NSGAII and TOPSIS for structural optimization of sandwich panels with corrugated core. *J Sandwich Struct Mater* 2014; 16: 398–417.
11. Li L, Zhao Z, Zhang R, et al. Dual-level stress plateaus in honeycombs subjected to impact loading: perspectives from bucklewaves, buckling and cell-wall progressive folding. *Acta Mech Sin* 2019; 35: 70–77.
12. Su P, Han B, Zhao Z, et al. Three-point bending of honeycomb sandwich beams with facesheet perforations. *Acta Mech Sin* 2018; 34: 667–675.
13. Wang L, Saito K, Gotou Y, et al. Design and fabrication of aluminum honeycomb structures based on origami technology. *J Sandwich Struct Mater* 2019; 21: 1224–1242.
14. Zhang H, Sun F, Fan H, et al. Free vibration behaviors of carbon fiber reinforced lattice-core sandwich cylinder. *Compos Sci Technol* 2014; 100: 26–33.
15. Li W, Sun F, Wang P, et al. A novel carbon fiber reinforced lattice truss sandwich cylinder: Fabrication and experiments. *Compos Part A Appl Sci Manuf* 2016; 81: 313–322.
16. Jiang S, Sun F, Fan H, et al. Fabrication and testing of composite orthogrid sandwich cylinder. *Compos Sci Technol* 2017; 142: 171–179.
17. Yang JS, Ma L, Chaves-Vargas M, et al. Influence of manufacturing defects on modal properties of composite pyramidal truss-like core sandwich cylindrical panels. *Compos Sci Technol* 2017; 147: 89–99.
18. Yang J, Xiong J, Ma L, et al. Study on vibration damping of composite sandwich cylindrical shell with pyramidal truss-like cores. *Compos Struct* 2014; 117: 362–372.
19. Fan H, Fang D, Chen L, et al. Manufacturing and testing of a CFRC sandwich cylinder with Kagome cores. *Compos Sci Technol* 2009; 69: 2695–2700.
20. Li W, Sun F, Wei W, et al. Fabrication and testing of composite corrugated-core sandwich cylinder. *Compos Sci Technol* 2018; 156: 127–135.
21. Su PB, Han B, Yang M, et al. Axial compressive collapse of ultralight corrugated sandwich cylindrical shells. *Mater Des* 2018; 160: 325–337.
22. Yang M, Han B, Su PB, et al. Axial crushing of ultralight all-metallic truncated conical sandwich shells with corrugated cores. *Thin Wall Struct* 2019; 140: 318–330.
23. Hemmatnezhad M, Rahimi GH, Tajik M, et al. Experimental, numerical and analytical investigation of free vibrational behavior of GFRP-stiffened composite cylindrical shells. *Compos Struct* 2015; 120: 509–518.
24. Belytschko T, Lin JJ and Chen-Shyh T. Explicit algorithms for the nonlinear dynamics of shells. *Comput Method Appl Mech Eng* 1984; 42: 225–251.
25. Mckay MD, Beckman RJ and Conover WJ. A comparison of three methods for selecting values of input variables in the analysis of output from a computer code. *Technometrics* 2000; 21: 55–61.

Appendix 1

Response surface functions for natural frequency and peak force

Full third-order response surface functions for F_1 and PF with are given in this appendix, as follows. Formula (3) is the expression of the first natural frequency (F_1) for CSSCC, formula (4) is the expression of the first natural frequency for TCSSCC, formula (5) is the expression of the peak force (PF) for CSSCC, and formula (6) is the expression of the peak force for TCSSCC.

$$\begin{aligned}F_{1-\mathrm{CSSCC}} = {} & -348.25 + 3295.941t_o + 2018.06t_\mathrm{i} - 169.65t_\mathrm{c} - 7129.99t_\mathrm{o}^2 - 4407.88t_\mathrm{i}^2 \\ & - 208.05t_\mathrm{c}^2 + 6201.99t_\mathrm{o}t_\mathrm{i} + 596.57t_\mathrm{o}t_\mathrm{c} + 18.52t_\mathrm{i}t_\mathrm{c} + 3596.24t_\mathrm{o}^3 \\ & + 1851.57t_\mathrm{i}^3 + 134.93t_\mathrm{c}^3 - 3026.35t_\mathrm{o}^2t_\mathrm{i} + 933.28t_\mathrm{o}^2t_\mathrm{c} - 527.12t_\mathrm{i}^2t_\mathrm{o} \\ & - 559.24t_\mathrm{i}^2t_\mathrm{c} - 945.46t_\mathrm{c}^2t_\mathrm{o} + 691.24t_\mathrm{c}^2t_\mathrm{i} - 350.63t_\mathrm{o}t_\mathrm{i}t_\mathrm{c}\end{aligned} \tag{3}$$

$$\begin{aligned}F_{1-\mathrm{TCSSCC}} = {} & -390.12 - 186.51t_o + 3816.65t_\mathrm{i} - 191.25t_\mathrm{c} - 465.47t_\mathrm{o}^2 - 2175.64t_\mathrm{i}^2 \\ & - 935.93t_\mathrm{c}^2 - 2201.37t_\mathrm{o}t_\mathrm{i} + 5359.83t_\mathrm{o}t_\mathrm{c} - 3622.37t_\mathrm{i}t_\mathrm{c} \\ & + 659.28t_\mathrm{o}^3 - 484.66t_\mathrm{i}^3 + 190.35t_\mathrm{c}^3 + 233.18t_\mathrm{o}^2t_\mathrm{i} - 3161.14t_\mathrm{o}^2t_\mathrm{c} \\ & + 2234.69t_\mathrm{i}^2t_\mathrm{o} + 812.13t_\mathrm{i}^2t_\mathrm{c} - 1014.51t_\mathrm{c}^2t_\mathrm{o} + 2250.56t_\mathrm{c}^2t_\mathrm{i} + 190.51t_\mathrm{o}t_\mathrm{i}t_\mathrm{c}\end{aligned} \tag{4}$$

$$\begin{aligned}PF_{\mathrm{CSSCC}} = {} & -6.63 + 33.19t_o - 0.17t_\mathrm{i} + 152.25t_\mathrm{c} + 49.30t_\mathrm{o}^2 + 38.93t_\mathrm{i}^2 - 113.72t_\mathrm{c}^2 \\ & + 60.74t_\mathrm{o}t_\mathrm{i} - 28.86t_\mathrm{o}t_\mathrm{c} + 53.29t_\mathrm{i}t_\mathrm{c} - 29.68t_\mathrm{o}^3 - 19.94t_\mathrm{i}^3 \\ & + 60.84t_\mathrm{c}^3 - 24.07t_\mathrm{o}^2t_\mathrm{i} + 19.94t_\mathrm{o}^2t_\mathrm{c} - 16.05t_\mathrm{i}^2t_\mathrm{o} + 2.11t_\mathrm{i}^2t_\mathrm{c} \\ & + 15.56t_\mathrm{c}^2t_\mathrm{o} - 36.34t_\mathrm{c}^2t_\mathrm{i} - 12.62t_\mathrm{o}t_\mathrm{i}t_\mathrm{c}\end{aligned} \tag{5}$$

$$\begin{aligned}PF_{\mathrm{TCSSCC}} = {} & -12.07 + 46.46t_o - 1.81t_\mathrm{i} + 158.19t_\mathrm{c} + 94.52t_\mathrm{o}^2 + 70.81t_\mathrm{i}^2 - 102.41t_\mathrm{c}^2 \\ & + 13.80t_\mathrm{o}t_\mathrm{i} - 74.27t_\mathrm{o}t_\mathrm{c} + 76.29t_\mathrm{i}t_\mathrm{c} - 70.60t_\mathrm{o}^3 - 32.66t_\mathrm{i}^3 \\ & + 55.04t_\mathrm{c}^3 + 19.62t_\mathrm{o}^2t_\mathrm{i} + 44.67t_\mathrm{o}^2t_\mathrm{c} - 18.71t_\mathrm{i}^2t_\mathrm{o} - 2.47t_\mathrm{i}^2t_\mathrm{c} \\ & + 24.99t_\mathrm{c}^2t_\mathrm{o} - 45.63t_\mathrm{c}^2t_\mathrm{i} - 18.33t_\mathrm{o}t_\mathrm{i}t_\mathrm{c}\end{aligned} \tag{6}$$